PROCEEDINGS OF SCIENCE

Meson Production in Au+Au Collisions at $\sqrt{s_{NN}} = 3.0$ GeV at STAR

Benjamin Kimelman[a,*] **for the STAR Collaboration**

[a] *University of California, Davis,*
1 Shields Ave, Davis CA, USA

E-mail: bkimelman@ucdavis.edu

In this proceedings, we present the first measurements of identified light and strange particle (π, K, ϕ) production in Au+Au collisions at $\sqrt{s_{NN}}$ = 3 GeV. Various models including thermal and transport model calculations are compared to data, which provide constraints to such models and indicate that the QCD matter produced in the 3 GeV fixed-target Au+Au collisons is considerably different from those at higher energies.

The International conference on Critical Point and Onset of Deconfinement - CPOD2021
15 – 19 March 2021
Online - zoom

*Speaker

PoS(CPOD2021)019

1. Introduction

Relativistic heavy ion collisions are a prime tool to probe the phase structure of strongly interacting matter under extreme conditions. The RHIC Beam Energy Scan II (BES-II) Program has three primary goals: searching for the onset of Quark-Gluon Plasma (QGP), studying the properties of produced QCD matter, and locating the possible QCD phase boundary and critical endpoint [1].

Particle production has long been used to investigate the properties of the produced QCD matter in heavy-ion collisions. The BES-II program covers a wide range of energies, including the transition from a hadronic dominated medium to a partonic dominated one. The BES-II program currently under way is designed to improve and extend upon the results from the BES-I program. Of particular interest is the high baryon density region which is accessible through the STAR fixed-target program, which has extended the energy reach from $\sqrt{s_{NN}}$ = 7.7 GeV to $\sqrt{s_{NN}}$ = 3.0 GeV. In these proceedings, the first measurements of charged particle and ϕ-meson production in Au + Au collisions at $\sqrt{s_{NN}}$ = 3.0 GeV will be presented.

2. Experiment

The data used in this analysis were collected in 2018 and was the first dataset of the official STAR Fixed-Target (FXT) program. A single beam with a total energy of 3.85 GeV/nucleon was steered 2 cm below the center of the vacuum pipe to collide with the top edge of a stationary gold target, providing Au+Au collisions at $\sqrt{s_{NN}}$ = 3.0 GeV. The gold target has a thickness of 0.25 mm (corresponding to a 1% nuclear interaction probability) and is located 200 cm to the west of the center of the STAR detector [2], directly at the edge of the Time Projection Chamber (TPC) [3]. The positioning and thickness of the target were optimized to balance the desire for large acceptance for tracking while minimizing pileup and energy loss in the target for all collision energies in the FXT program. For Au+Au FXT collisions at $\sqrt{s_{NN}}$ = 3.0 GeV, midrapidity lies at 1.05 in the laboratory frame, which falls in the middle of the STAR detector providing excellent particle tracking and identification capabilities.

The main detectors used in this analysis were the TPC and the Barrel Time of Flight (bTOF) detector [4]. Additionally, the trigger was provided by a signal in the east Beam-Beam Counter (BBC) and at least five hits in the bTOF detector. In total, approximately 2.6×10^8 minimum bias (MB) triggered events are used in this analysis.

Tracking and particle identification (PID) are done using the energy loss (dE/dx) information from the TPC and time of flight ($1/\beta$) from the bTOF. Pions and kaons are identified directly using their dE/dx and $1/\beta$ whereas ϕ mesons are reconstructed through the hadronic decay channel, $\phi \rightarrow K^+ + K^-$, where combinatioral background is estimated using the mixed event technique [5]. Figure 1 shows the ϕ meson invariant mass distribution for the 0-60% most central collisions.

3. Light and Strange Hadron Yields

Raw yields of pions and kaons are obtained by fitting the dE/dx and $1/\beta$ distributions, while the ϕ meson yields are obtained by fitting K^+ and K^- invariant mass distributions. TPC tracking

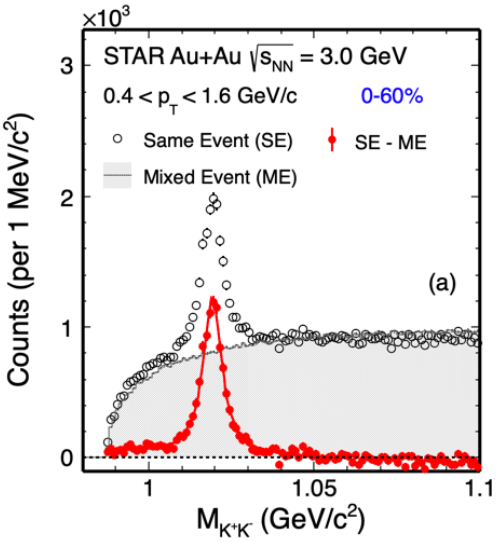

Figure 1: ϕ meson invariant mass peak reconstructed from the hadronic channel for the 0-60% most central Au+Au collisions at $\sqrt{s_{NN}}$ = 3.0 GeV.

and acceptance efficiencies are then obtained by embedding simulated tracks into real data and running that through a full GEANT simulation of the STAR detector to understand its response. Corrections to these efficiencies, along with a data-derived bTOF matching efficiency, are applied to the data to produce the invariant spectra.

The pions are fit with double-thermal functions, each of the form

$$\frac{1}{2\pi m_T}\frac{d^2N}{dm_T\,dy} = Am_T e^{-(m_T-m_0)/T}. \tag{1}$$

Each thermal function describes pion production through different mechanisms. The thermal function at low $m_T - m_0$ corresponds to a low temperature and describes the production of pions through the decay of the Δ resonance, whereas the thermal function at high $m_T - m_0$ corresponds to a high temperature and describes the thermal production of pions. This two-component functional form was shown by the E895 Collaboration to provide a good description of the data [6] and is thus used in this analysis which has a very similar center of mass energy. This functional form with two components is necessary at this low energy as a significant amount of the pions are produced in the decay of the Δ resonance.

The kaons and ϕ-mesons are fit with m_T-exponential functions (Eq. 2), which indicate the thermal nature of their production.

$$\frac{1}{2\pi m_T}\frac{d^2N}{dm_T\,dy} = Ae^{-(m_T-m_0)/T}. \tag{2}$$

The fits of the spectra are integrated over $m_T - m_0$ in order to obtain the rapidity density distributions. Figure 2 shows the charged meson rapidity density distributions for the 0-5% most central collisions while Fig. 3 shows the ϕ-meson and K^- rapidity density distributions for various collision centralities.

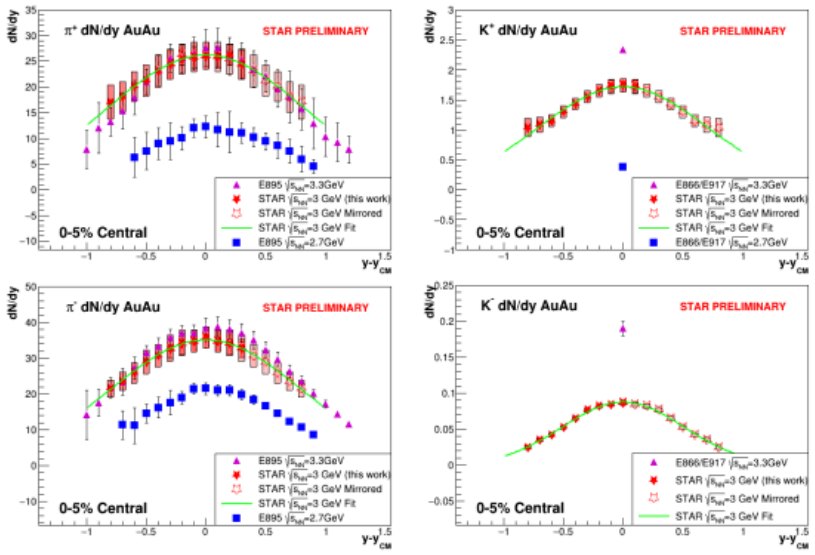

Figure 2: Charged meson rapidity density distributions for the 0-5% most central collisions compared to measurements from various experiments at the AGS. π^+ (top left) and π^- (bottom left) are compared with measurements from the E895 experiment [6], while K^+ (top right) and K^- (bottom right) are compared with measurements from the E866 and E917 experiments [7]. Statistical (bars) and systematic (boxes) uncertainties are shown.

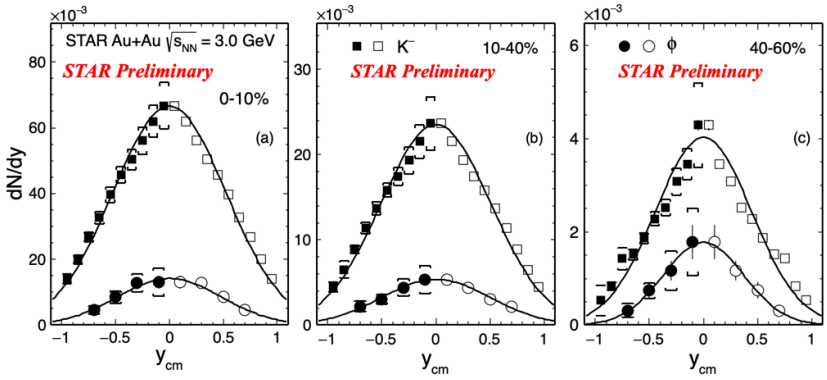

Figure 3: ϕ-meson and K^- rapidity density distributions for various collision centralities. Statistical (bars) and systematic (brackets) uncertainties are shown.

From the particle spectra and rapidity density distributions, various particle production mechanisms and other physical effects can be observed including the Coulomb potential modifying the pion spectra, associated production of the K^+, and local strangeness conservation with the ϕ-meson.

3.1 Coulomb Potential

In heavy-ion collisions at these low energies, baryon stopping causes a non-negligible positive charge of the interaction region. This positive charge can modify the spectra of particles through the Coulomb interaction, which is most evident in the charged pions due to their small mass. A simple model which incorporates the Bose-Einstein nature of pions and the radial expansion of the

fireball is used to fit the midrapidity π^+/π^- spectra in order to extract the Coulomb potential (V_C) and initial pion ratio (R_{init}) [8], as can be seen in Fig. 4.

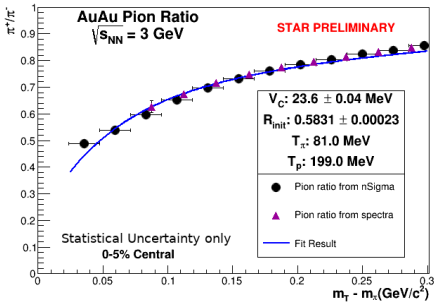

[t]

Figure 4: Ratio of midrapidity π^+/π^- spectra. These data are fit with a model as described in the text which is used to extract the Coulomb potential of the fireball and the initial pion ratio.

From this measurement, a comparison is made to global trends [8]. Figure 5 shows this comparison, where this measurement agrees very well with the trend seen in both quantities. The upper panel of Fig. 5 includes midrapidity net-proton dN/dy measurements with an empirical fit, matching closely with the measurements of the Coulomb potential. The lower panel of Fig. 5 includes a fit to the data which indicates a smooth transition from the Δ resonance dominating pion production at low collision energies to the predominance of thermal production at higher energies.

3.2 Kaon Production

Due to the strange quarks they contain, all kaons measured must have been produced as a result of the heavy-ion collisions being studied. At high energies, most kaons are produced thermally, where a K^+ and K^- are produced as a pair to conserve strangeness. At the low energy being studied here, thermal production still exists but it is dominated by the production of K^+ in association with the Λ baryon ($N + N \rightarrow N + \Lambda + K^+$). By looking at the ratio of midrapidity K^-/K^+, the fraction of thermally produced K^+ can be observed, as seen in Fig. 6.

The predominance of the associated production mechanism of the K^+ reinforces the baryon-dominated nature of the collisions at $\sqrt{s_{NN}}$ = 3.0 GeV. Additionally, the lack of such a production mechanism for K^- in association with the $\bar{\Lambda}$ anti-baryon further supports this conclusion.

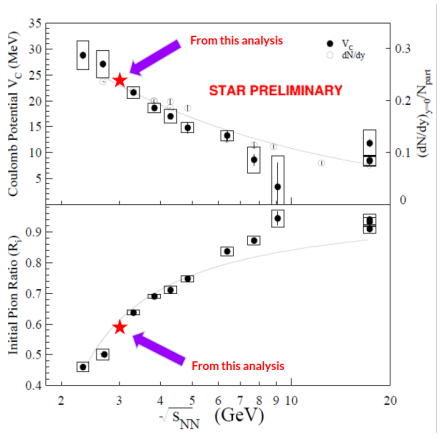

Figure 5: Coulomb potential (top) and initial pion ratio (bottom) data extracted from a model of the pion ratio. The measurement in this analysis agrees well with the trend seen from SIS, AGS, and SPS measurements [8].

3.3 ϕ-meson Strangeness Conservation

In the low energy collisions at hand, strangeness production is rare and it has been argued that strangeness number needs to be conserved locally on an event-by-event basis described by the Canonical Ensemble (CE), which leads to a reduction in the yields of hadrons with non-zero strangeness number. Furthermore, with this energy just above the ϕ-meson production threshold, the strangeness production mechanisms are expected to be different from at higher energies. Figure 7 shows the ratio of ϕ/K^- for various collision centralities. This is a precise measurement compared to previous studies, with

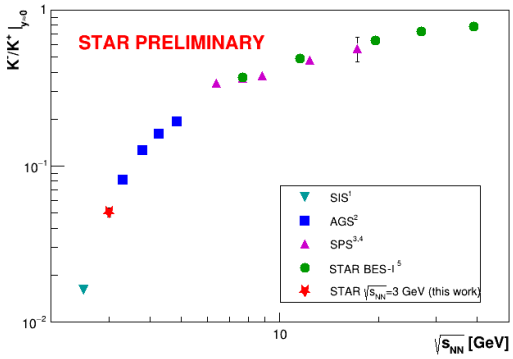

Figure 6: Midrapidity K^-/K^+ yield (dN/dy) as a function of center-of-mass energy [7, 9–11]. This ratio can be seen as the fraction of K^+ that are produced thermally compared to in association with the Λ baryon. Only $\sim 5\%$ of K^+ are produced thermally at $\sqrt{s_{NN}}$ = 3.0 GeV. Statistical uncertainties only are shown.

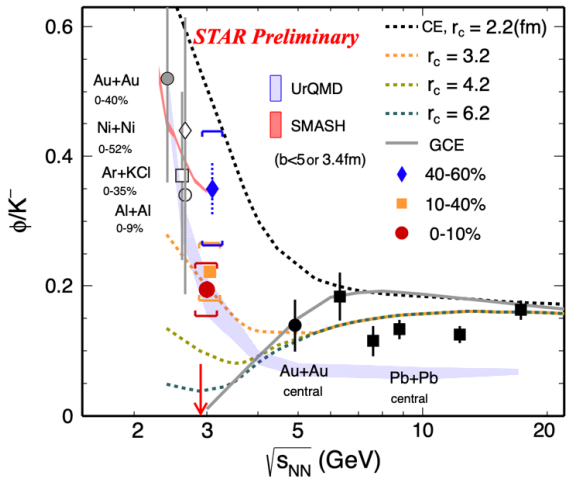

Figure 7: ϕ/K^- yield as a function of center-of-mass energy. Comparisons to various transport and thermal models are made and trends can be observed between measurements from other experiments [5]. Statistical (bars) and systematic (brackets) uncertainties are shown.

the ratios for the 0-10% and 10-40% centralities being $\sim 5\sigma$ larger than zero.

Furthermore, these results have been compared to various statistical and transport model calculations. The Grand Canonical Ensemble (GCE) clearly underestimates this ratio since it only conserves strangeness on average. In contrast, the Canonical Ensemble (CE), which conserves strangeness locally on a strangeness correlation length (r_c), agrees better with the observed data. Additionally, transport models with resonance decays, including UrQMD and SMASH, can reasonably describe the data.

4. Summary

In Au+Au collisions at $\sqrt{s_{NN}}$ = 3.0 GeV, it has been shown that the dominant particle production mechanisms are different from what is seen at high energy. Pion production has a significant contribution from decays of the Δ resonance while the majority of K^+ are produced in association with the Λ baryon. The ϕ/K^- ratio rules out the GCE and favors the CE which locally conserves strangeness. These observations indicate changes in particle production, in particular to strangeness production, and the EoS of dense baryon matter.

Acknowledgments

This material is based upon work supported by the National Science Foundation under Grant No. 1812398 (Cebra and Calderón de la Barca). Any opinions, findings, and conclusions or recommendations expressed in this material are those of the authors and do not necessarily represent the views of the National Science Foundation.

References

[1] STAR collaboration, *Studying the phase diagram of QCD matter*, *SN0598* (2014) .

[2] STAR collaboration, *STAR detector overview*, *Nucl. Instrum. Meth. A* **499** (2003) 624.

[3] M. Anderson, J. Berkovitz, W. Betts, R. Bossingham, F. Bieser, R. Brown et al., *The STAR time projection chamber: a unique tool for studying high multiplicity events at RHIC*, *Nuc. Instrum. Meth. A* **499** (2003) 659.

[4] STAR collaboration, *Multigap RPCs in the STAR experiment at RHIC*, *Nucl. Instrum. Meth. A* **661** (2012) S110.

[5] STAR collaboration, *Probing strangeness canonical ensemble with K^-, $\phi(1020)$ and Ξ^- production in Au+Au collisions at $\sqrt{s_{NN}}$ = 3 GeV*, arXiv/2108.00924.

[6] E895 collaboration, *Charged pion production in 2A to 8AGeV central Au + Au collisions*, *Phys. Rev. C* **68** (2003) 054905.

[7] E866/E917 collaboration, *An excitation function of K^- and K^+ production in Au+Au reactions at the ags*, *Physics Letters B* **490** (2000) 53.

[8] D. Cebra, S.G. Brovko, C.E. Flores, B.A. Haag and J.L. Klay, *Coulomb effect in Au+Au and Pb+Pb collisions as a function of collision energy*, arXiv/1408.1369.

[9] KaoS collaboration, *Kaon and antikaon production in heavy ion collisions at 1.5 AGeV*, *Journal of Physics G: Nuclear and Particle Physics* **28** (2002) 2011.

[10] NA49 collaboration, *Pion and kaon production in central* Pb + Pb *collisions at* 20*A and* 30*A GeV: Evidence for the onset of deconfinement*, *Phys. Rev. C* **77** (2008) 024903.

[11] STAR Collaboration collaboration, *Bulk properties of the medium produced in relativistic heavy-ion collisions from the beam energy scan program*, *Phys. Rev. C* **96** (2017) 044904.